Modeling Earth Systems and Environment (2025)11:246
https://doi.org/10.1007/s40808-025-02417-9

ORIGINAL ARTICLE

Modeling prevalence of meningitis control strategies through evaluating with available data on meningitis cases reported in Nigeria

Olumuyiwa James Peter[1,2,3] · Festus Abiodun Oguntolu[4] · Nkuba Nyerere[5] · A. El-Mesady[6]

Received: 29 August 2024 / Accepted: 6 April 2025

Abstract

Meningitis is a major public health concern, especially in developing nations, due to its devastating consequences for human health. Although modeling studies have examined disease transmission dynamics, little attention has been paid to how control strategies affect the behavior of different population groups, including carriers, symptomatic individuals, hospitalized patients, and those in intensive care. This study proposes a computational framework that compares the effectiveness of vaccination of people at risk of the disease versus treating symptomatic infected persons. The basic reproduction number is used to evaluate the equilibrium points. Assess the precision of the proposed model's illustration to data. We fit the meningitis model using the information at our disposal on meningitis cases reported in Nigeria from the first week of January to the last week of December 2023; this was obtained from the Nigerian Center for Disease Control (NCDC) database. We also performed a sensitivity analysis using a normalized forward sensitivity index to see which parameters had significant effects on the effective reproduction number. The results of both analytical techniques and numerical simulations reveal that recruitment rate, vaccination, progression from carrier to symptomatic stages, and disease-induced death all significantly reduce the incidence and prevalence of meningitis in the community. The study findings could be used to inform decisions about meningitis control initiatives.

Keywords Meningitis · Reproduction number · Stability analysis · Control measures · Model simulations

Mathematics Subject Classification 34A08 · 34D05 · 97M60 · 92-10 · 37M05

Introduction

A dangerous infection of the meninges, the delicate and protective membranes encircling the brain and spinal cord, is known as meningitis (Organization 2003; Putz et al. 2013). Numerous infections, such as bacteria, fungi, and viruses, can cause meningitis; nevertheless, bacterial meningitis is the most prevalent type globally. Over 70% of disease infections are caused by three main bacteria: *Neisseria meningitidis*, *Haemophilus influenzae*, and *Streptococcus pneumoniae*. Of these, *Neisseria*

✉ Olumuyiwa James Peter
peterjames4real@gmail.com

Festus Abiodun Oguntolu
festus.tolu@futminna.edu.ng

Nkuba Nyerere
emmankuba@sua.ac.tz

A. El-Mesady
ahmed.ibrahiem81@el-eng.menofia.edu.eg

[1] Present Address: Department of Mathematics, Saveetha School of Engineering, SIMATS, Saveetha University, Chennai 602105, Tamil Nadu, India

[2] Department of Mathematical and Computer Sciences, University of Medical Sciences, Ondo City, Ondo State, Nigeria

[3] Department of Epidemiology and Biostatistics, School of Public Health, University of Medical Sciences, Ondo City, Ondo State, Nigeria

[4] Department of Mathematics, Federal University of Technology Minna, Minna, Niger State, Nigeria

[5] Department of Mathematics and Statistics, Sokoine University of Agriculture, Morogoro, Tanzania

[6] Department of Physics and Engineering Mathematics, Faculty of Electronic Engineering, Menoufia University, Menouf 32952, Egypt

Published online: 14 May 2025

meningitidis is the most important because of its high morbidity and mortality rates as well as its capacity to start epidemics. Epidemics can be caused by six of the twelve identified serogroups of *N. meningitidis* (A, B, C, W, X, and Y) (WHO 2023). The illness can have catastrophic consequences and is a significant public health concern (Young and Thomas 2018). Direct contact between susceptible people and sick people, particularly droplets of respiratory or throat secretions from an infected person, is how meningitis is spread. Transmission is also facilitated by variables like smoking and crowding, as well as by extended close encounters like kissing, living in close quarters with an infected person, coughing on someone, and sneezing. The average incubation period is 4 days but can range from 2 to 10 days (NCDC 2019).

The most common signs and symptoms include fever, headache, nausea, vomiting, photophobia (sensitivity to bright lights), neck stiffness, and altered levels of consciousness. In younger children, these signs may be harder to detect, and symptoms such as irritability, poor feeding, and inactivity are often observed. N. meningitidis can also lead to meningococcal septicemia, which manifests as fatigue, severe muscle pain, vomiting, cold extremities, rapid breathing, low blood pressure, and a purpuric (dark purple, non-blanching) rash (Young and Thomas 2018; NCDC 2019).

With incidence rates that range from about 0.9 per 100,000 people yearly in high-income countries to 80 per 100,000 people annually in low-income countries, bacterial meningitis is a serious health hazard on a global scale. The disease has a mortality rate of up to 54% in low-income areas. Additionally, up to 24% of survivors may suffer from focal neurological abnormalities or hearing loss, among other long-term neurological consequences (Oordt-Speets et al. 2018). Bacterial meningitis is still a major public health concern in Africa. The disease has already moved beyond these historical borders, impacting more forested areas in the middle parts of the continent, while once being centered in the "Meningitis Belt" with Sub-Saharan and Sudanian environmental conditions (Mazamay et al. 1928). In addition to outbreaks, at least 1.2 million instances of bacterial meningitis are thought to happen annually, with 135,000 of those cases ending in death. Of these, meningococci are responsible for about 500,000 cases and 50,000 fatalities (Verma and Khanna 2012).

The intricate dynamics of many diseases are commonly explained by mathematical models (Myrzakerimova et al. 2024; Nyerere et al. 2024). These models help researchers predict future outbreaks, identify key factors influencing transmission, and comprehend how diseases spread among communities (Ijeh et al. 2024; Asplin et al. 2024; Richard and Lipsitch 2024; Saravanan et al. 2024; Asamoah et al. 2020; Peter et al. 2022, 2023a, 2023b; James Peter et al. 2022; Ojo et al. 2023; Abioye et al. 2020, 2021, 2024). To investigate the patterns of transmission of meningitis infections in humans, a number of models have been developed. Toaha et al. investigated the efficacy of several strategies in controlling the spread of meningitis (Toaha and Azis 2025). According to the study's findings, vaccination, public awareness initiatives, and therapeutic interventions can all help stop the spread of meningitis. A study by Hadley et al. (2024) aimed to develop and evaluate control measures for pneumococcal meningitis outbreaks in the African Meningitis Belt. According to the study, the introduction of pentavalent vaccines led to a notable decrease in the number of carriers, which is helpful in reducing the prevalence of the disease.

A study by Crankson et al. (2023) evaluated how well vaccinations work to restrict the dynamics of bacterial meningitis transmission. According to a study, if at least 25 Employing data from Yobe State Specialist Hospital in Damaturu, Nigeria, Madaki et al. (2023) developed a mathematical model to assess the dynamics of bacterial meningitis, specifically meningococcal meningitis. The study found that in order to effectively counteract the effect of vaccination on meningitis, a higher incidence of infection transmission requires a higher rate of vaccination and treatment. Opoku and associates (Opoku et al. 2022) discussed their work on cost-effectiveness analysis and modelling the dynamics of meningitis transmission in Ghana's high- and low-risk populations. The study came to the conclusion that the best method of controlling meningitis is to combine therapy and vaccination. Cost-effectiveness study, however, reveals that these tactics are among the priciest to implement. Therefore, it is essential to promote personal protection, which is a more economical option, particularly for people moving from areas with low to high meningitis risk.

In order to examine the dynamics of meningococcal meningitis transmission, Musa et al. (2020) developed an epidemic model that distinguished between susceptible populations at high and low risk according to the accessibility of medical care. According to analysis, the model shows backward bifurcation. The results emphasize that in order to lower illness incidence and death, communities-especially those in endemic areas-need to have access to quality medical care. To study the dynamics of meningitis, Peter et al. (2022) created a mathematical model based on the Atangana Baleanu Caputo derivative. The benefits of using fractional calculus to model real-world issues were discussed. The asymptotic stability requirements for endemic and meningitis-free equilibria were established on a local and global level. The model's backward bifurcation was demonstrated.

A mathematical framework for co-infection between malaria and meningitis in kids under five years old was

developed and examined by Maseno (2011). The study found that lowering the number of new co-infection cases and lowering the number of malaria infection cases, either through prevention or prompt, efficient treatment, depends on the socioeconomic position of a community. A deterministic model was presented by Veronica et al. (2021) to study the transmission of meningitis: susceptible, vaccinated, carrier, infected, treated, and recovered. According to the study's findings, vaccination is essential for disease prevention. Furthermore, reducing the values of components with a negative sensitivity index will help to limit the spread of disease, according to sensitivity analysis of the reproduction number.

A deterministic approach was developed by Chukwu et al. (2020) to describe the dynamics of co-infection between listeriosis and meningitis. Both the co-infection model and each of its submodels undergo mathematical analysis. According to the results of the numerical simulations, the rate of co-infections between Listeriosis and Meningitis is decreased when the environment's Listeria bacteria is reduced and the recovery rate for Meningitis is raised. A mathematical model was presented by Elmojtaba and Adam (2017) to investigate the dynamics of meningitis. Studies indicate that this model was used to gain a better understanding of how a vaccination would affect a small human population. The results of the study showed that if vaccination uptake was high, the disease might be under control.

To comprehend the changing patterns of bacterial meningitis in a population, Asamoah et al. (2018) created a nonlinear deterministic model with time-dependent controls. The simulation shows a globally asymptotically stable endemic equilibrium and a unique globally asymptotically stable disease-free equilibrium when the effective reproduction number is smaller than one. The model shows a transcritical bifurcation when the reproduction number is equal to one. The study also found that the best way to control bacterial meningitis is to combine vaccination with other therapies, and that carriers were more likely to spread the infection than people with clinical symptoms.

Kotola and Mekonnen (2022) examined effective interventions for meningitis and pneumonia coinfection using a deterministic mathematical model and offered logical suggestions to program implementers, policymakers, and public health. The study found that the co-infected mouse had an effective reproduction number of fewer than one due to the effective reproduction numbers of pneumonia and meningitis. According to numerical simulations, treatment, less contacts with infectious people, and increased immunization against the two diseases significantly reduced disease in communities.

Meningitis is a significant issue in the modern world despite a great deal of research on its mechanics of transmission and management. Frequent outbreaks around the globe emphasize the need for continuous monitoring, prompt action, and improved access to vaccines and alternate treatments. Nigeria has documented numerous cases of bacterial meningitis, particularly in the "meningitis belt," which is a region spanning sub-Saharan Africa. Nigeria's weekly epidemiological trend of meningitis incidence between 2020 and 2023 Fig. 1 shows how changes in case numbers may be influenced by seasonal patterns, vaccination campaigns, and public health initiatives.

Effective disease control and preventive measures depend on an understanding of these trends. The purpose of this study is to present a comprehensive analysis of the epidemiological patterns of meningitis in Nigeria, with the goal of improving disease management techniques and influencing public health policy. The structure of this paper is as follows: The model's formulation is covered in Sect. 2, while Sect. 3 derives the model's fundamental characteristics. Section 4 presents the numerical results, whereas Sect. 5 discusses the analytical findings and conclusion.

Model formulation

Let the overall population size at time t be represented by $N(t)$. The population is separated into seven different groups according on each person's epidemiological status. Meningitis-susceptible people are represented by $S(t)$ and meningitis-vaccinated people by $V(t)$. Carrier class $C(t)$ includes individuals infected with the meningitis pathogen but not exhibiting symptoms; they can unknowingly spread the infection to others. The intensive care compartment $I_c(t)$ includes patients with severe cases of meningitis who require intensive medical care. These individuals might have life-threatening complications such as sepsis or increased intracranial pressure. Treatment of individuals in this category involves mechanical ventilation, aggressive antibiotic therapy, and neurological monitoring to manage critical conditions. The infected class $I(t)$ represents individuals who are symptomatic and infected with meningitis. The hospitalization class $H(t)$ comprises individuals who have developed severe symptoms of meningitis and require medical care in a hospital setting. The recovered class $R(t)$ includes individuals who have recovered from meningitis; however, recovered individuals may lose immunity and become susceptible again. It is assumed that the vaccine is not 100% effective; therefore, vaccinated individuals may become exposed to meningitis, reducing the vaccinated population by infection at the rate $(1-\eta)\alpha$, where η represents vaccine efficacy. Thus, if $\eta = 1$, this implies that the vaccine is 100% effective, so $0 \leqslant \eta \leqslant 1$. It is assumed

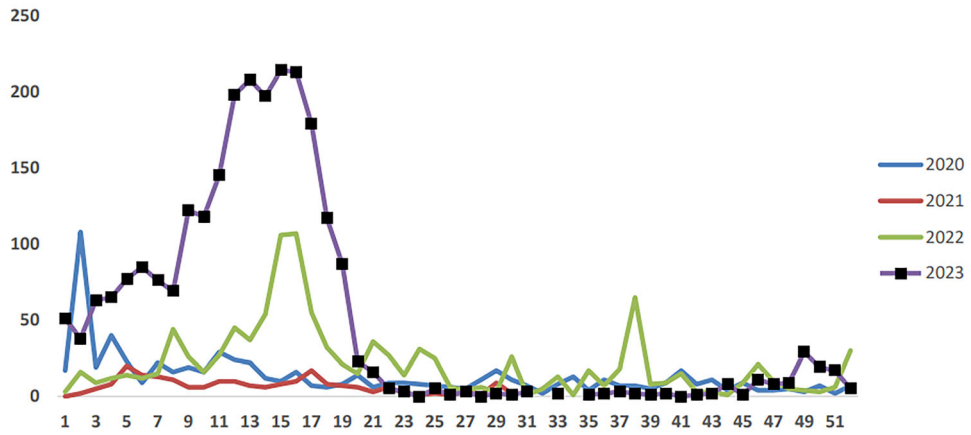

Fig. 1 Weekly epidemiological trend of Meningitis cases in Nigeria from 2020 to 2023. Source: NC (2024)

that individuals in the carrier class progress to the symptomatic infected class $I(t)$ at a rate τ or recover naturally at a rate γ_c. Meningitis, particularly bacterial meningitis, often necessitates hospitalization and intensive care due to its potentially life-threatening nature and rapid progression. Hospitalization allows for immediate diagnosis and initiation of antibiotic or antiviral treatments, which are critical for preventing severe complications and reducing mortality. Patients require continuous monitoring of vital signs and neurological status to manage symptoms such as fever, headache, neck stiffness, and altered mental status. Additionally, the hospital setting enables prompt intervention for complications like seizures, hearing loss, and hydrocephalus. In severe cases, the infection can cause sepsis and increased intracranial pressure, necessitating advanced life support and neurological monitoring available in an ICU. Intensive care is essential for managing severe infections, preventing organ failure, and providing life-saving interventions. Therefore, the critical care provided in hospitals and ICUs is vital for effectively managing meningitis and improving patient outcomes (degli Atti et al. 2014; Meyfroidt et al. 2020; Hinduja et al. 2019).

Our assumption is that those in the symptomatic infected class $I(t)$ can either recover spontaneously at a rate γ_i or move on to the hospitalized class at a rate ε. The recovery rate from hospitalization is represented by γ_h and the recovery rate from intensive care by γ_{ic}. The progression rate from the hospitalized class $H(t)$ to the intensive care unit $I_c(t)$ is represented by θ.

The susceptible class $S(t)$ population grows steadily at a rate ϕ, maybe as a result of immigration or births, and is vaccinated at a rate α_1 while losing immunity at a rate α_2. At a rate σ, recovered individuals lose their immunity and become susceptible again.

The population of the susceptible class is reduced due to effective contact with infected individuals at a rate $\alpha(t)$, defined by:

$$\alpha(t) = \beta(\rho C + I + H + I_c)$$

where β is the effective contact rate. The infectivity of individuals in the carrier class is indicated by ρ, which is a modification parameter for the carrier class. This is because carriers are more likely to spread the virus as they are unaware of their condition.

In every class, natural death occurs at a rate μ. We assume a uniform disease-induced death rate δ for patients in the intensive care class $I_c(t)$, hospitalized class $H(t)$, and symptomatic infected class $I(t)$.

These concepts are illustrated by sets of nonlinear differential equations in (1), while a graphical representation of the model is given in Fig. 2 (see Table 1).

$$\begin{aligned}
\frac{dS}{dt} &= \phi - \alpha(t)S + \sigma R + \alpha_2 V - (\alpha_1 + \mu)S,\\
\frac{dV}{dt} &= \alpha_1 S - (1-\eta)\alpha(t)V - (\alpha_2 + \mu)V,\\
\frac{dC}{dt} &= \alpha(t)S + (1-\eta)\alpha(t)V - (\gamma_c + \mu + \tau)C,\\
\frac{dI}{dt} &= \tau C - (\mu + \delta + \varepsilon + \gamma_i)I,\\
\frac{dH}{dt} &= \varepsilon I - (\mu + \delta + \theta + \gamma_h)H,\\
\frac{dI_C}{dt} &= \theta H - (\mu + \delta + \gamma_{ic})I_c,\\
\frac{dR}{dt} &= \gamma_h H + \gamma_i I + \gamma_{ic} I_c + \gamma_c C - \sigma R.
\end{aligned} \tag{1}$$

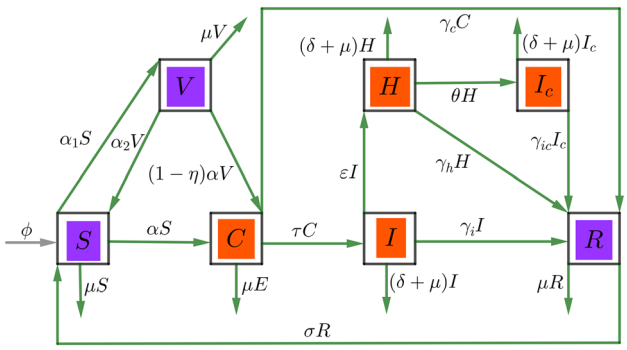

Fig. 2 Flow Chart of the proposed model as given in (1)

Table 1 An explanation of the variables and parameters of the meningitis model

Variable	Description
$S(t)$	Susceptible individuals
$V(t)$	Vaccinated individuals
$C(t)$	Carrier class (asymptomatic carriers)
$I(t)$	Symptomatic infected individuals
$H(t)$	Hospitalized individuals
$I_c(t)$	Intensive care patients
$R(t)$	Recovered individuals
$N(t)$	Total population size
Parameter	**Description**
ϕ	Recruitment rate into susceptible class (e.g., due to births)
α_1	Vaccination rate
α_2	Rate of loss of immunity in susceptible individuals
β	Effective contact rate
ρ	Modification parameter for carrier class infectivity
τ	Rate of progression from carrier class to symptomatic infected class
ε	Rate of progression from symptomatic infected class to hospitalization
γ_c	Recovery rate from carrier class
γ_i	Recovery rate from symptomatic infected class
γ_h	Recovery rate from hospitalization
γ_{ic}	Recovery rate from intensive care
σ	Rate of loss of immunity in recovered individuals
μ	Natural death rate
δ	Disease-induced death rate
θ	Progression rate from hospitalised class to intensive care class
η	Vaccine efficacy (reduction in infection rate for vaccinated individuals)

Model analysis

Theorem 3.1 *The area* $\Omega_+ = \{(S, V, C, I, H, I_c, R), S > 0, V \geqslant 0, C \geqslant 0, I \geqslant 0, H \geqslant 0, I_c \geqslant 0, R \geqslant 0\}$ *is a positive invariant for the model system* (1).

Proof From the model system (1), we have

$$\begin{cases} \frac{dS}{dt}|_{S=0} = \phi + \sigma R + \alpha_2 V > 0, \\ \frac{dV}{dt}|_{V=0} = \alpha_1 S > 0, \\ \frac{dC}{dt}|_{C=0} = \alpha(t)S + (1-\eta)\alpha(t)V > 0, \\ \frac{dI}{dt}|_{I=0} = \tau C \geqslant 0, \\ \frac{dH}{dt}|_{H=0} = \varepsilon I \geqslant 0, \\ \frac{dI_c}{dt}|_{I_c=0} = \theta H \geqslant 0, \\ \frac{dR}{dt}|_{R=0} = \gamma_h H + \gamma_i I + \gamma_{ic} I_c + \gamma_c C \geqslant 0. \end{cases} \tag{2}$$

As a consequence, the solution will consistently stay within the boundaries of Ω_+. □

To analyze the meningitis model and determine the feasible region where the total population remains bounded, follow these steps:

Let the total human population be defined as:

$$N(t) = S(t) + V(t) + C(t) + I(t) + H(t) + I_c(t) + R(t).$$

From the model equations, we compute the derivative of N:

$$\frac{dN}{dt} = \frac{dS}{dt} + \frac{dV}{dt} + \frac{dC}{dt} + \frac{dI}{dt} + \frac{dH}{dt} + \frac{dI_c}{dt} + \frac{dR}{dt}. \tag{3}$$

Substituting from equations (1), we get:

$$\begin{aligned} \frac{dN}{dt} &= (\phi - \alpha(t)S + \sigma R + \alpha_2 V - (\alpha_1 + \mu)S) \\ &\quad + (\alpha_1 S - (1-\eta)\alpha(t)V - (\alpha_2 + \mu)V) \\ &\quad + (\alpha(t)S + (1-\eta)\alpha(t)V - (\gamma_c + \mu + \tau)C) \\ &\quad + (\tau C - (\mu + \delta + \varepsilon + \gamma_i)I) \\ &\quad + (\varepsilon I - (\mu + \delta + \theta + \gamma_h)H) \\ &\quad + (\theta H - (\mu + \delta + \gamma_{ic})I_c) \\ &\quad + (\gamma_h H + \gamma_i I + \gamma_{ic} I_c + \gamma_c C - \sigma R). \end{aligned}$$

Simplifying, we obtain:

$$\frac{dN}{dt} = \phi - \mu N - \delta I.$$

From this differential equation, we derive the inequality:

$$\frac{dN}{dt} \leqslant \phi - \mu N. \tag{4}$$

Integrating (4) from 0 to t:

$$\int_0^t \frac{dN}{\phi - \mu N} \leqslant \int_0^t dt,$$
$$-\frac{1}{\mu}\ln(\phi - \mu N)\Big|_0^t \leqslant t.$$

Exponentiating both sides gives:

$$\frac{\phi - \mu N(t)}{\phi - \mu N(0)} \geqslant e^{-\mu t}.$$

Rearranging for $N(t)$:

$$N(t) \leqslant \frac{\phi}{\mu} - \left(\frac{\phi - \mu N(0)}{\mu}\right) e^{-\mu t}.$$

Therefore, the feasible region for the meningitis model, ensuring that the total population $N(t)$ does not exceed $\frac{\phi}{\mu}$, is:

$$\Gamma = \left\{(S(t), V(t), C(t), I(t), H(t), I_c(t), R(t)) \in \mathbb{R}^7 : 0 < N(t) \leqslant \frac{\phi}{\mu}\right\}.$$

Analysis of equilibrium point stability

The methodology used to derive the equilibrium points (EPs) of the model described by (1) is presented here. The process begins with the identification of the EPs, followed by an assessment of the model's stability. The determination of the equilibria for the model in (1) involves solving the following set of equations:

$$\begin{cases} \phi - \alpha(t)S + \sigma R + \alpha_2 V - (\alpha_1 + \mu)S = 0, \\ \alpha_1 S - (1-\eta)\alpha(t)V - (\alpha_2 + \mu)V = 0, \\ \alpha(t)S + (1-\eta)\alpha(t)V - (\gamma_c + \mu + \tau)C = 0, \\ \tau C - (\mu + \delta + \varepsilon + \gamma_i)I = 0, \\ \varepsilon I - (\mu + \delta + \theta + \gamma_h)H = 0, \\ \theta H - (\mu + \delta + \gamma_{ic})I_C = 0, \\ \gamma_h H + \gamma_i I + \gamma_{ic} I_C + \gamma_c C - \sigma R = 0. \end{cases} \tag{5}$$

Hence, we obtain the disease-free EP; $E_0 = (S^*, V^*, C^*, I^*, H^*, I_c^*, R^*)$ that can be represented by

$$\begin{cases} S^* = \dfrac{\phi(\alpha_2 + \mu)}{\mu(\alpha_1 + \alpha_2 + \mu)} > 0, \\ V^* = \dfrac{\alpha_1 \phi}{\mu(\alpha_1 + \alpha_2 + \mu)} > 0, \\ C^* = 0, \\ I^* = 0, \\ H^* = 0, \\ I_c^* = 0, \\ R^* = 0. \end{cases} \tag{6}$$

The basic reproduction number, denoted as R_0, is typically calculated using the next-generation matrix method proposed by Diekmann et al. (1990), Van den Driessche and Watmough (2002), Van den Driessche (2017) and implemented in Nyerere and Liana (2024), Ruoja et al. (2025). This approach allows us to express R_0 as follows:

$$R_0 = \rho(FV^{-1}), \tag{7}$$

Assuming that F and V are defined as follows, where ρ represents the spectral radius of the matrix FV^{-1}:

$$F = \begin{pmatrix} \beta\rho(S^* + (1-\eta)V^*) & \beta(S^* + (1-\eta)V^*) & \beta(S^* + (1-\eta)V^*) & \beta(S^* + (1-\eta)V^*) \\ 0 & 0 & 0 & 0 \\ 0 & 0 & 0 & 0 \\ 0 & 0 & 0 & 0 \end{pmatrix}, \tag{8}$$

$$V = \begin{pmatrix} \gamma_c + \mu + \tau & 0 & 0 & 0 \\ -\tau & \delta + \varepsilon + \gamma_i + \mu & 0 & 0 \\ 0 & -\varepsilon & \delta + \gamma_h + \theta + \mu & 0 \\ 0 & 0 & -\theta & \delta + \gamma_{ic} + \mu \end{pmatrix}. \tag{9}$$

Thus, we have

$$V^{-1} = \begin{pmatrix} \frac{1}{\gamma_c+\mu+\tau} & 0 & 0 & 0 \\ \frac{\tau}{(\gamma_c+\mu+\tau)(\delta+\varepsilon+\gamma_i+\mu)} & \frac{1}{\delta+\varepsilon+\gamma_i+\mu} & 0 & 0 \\ \frac{\varepsilon\tau}{(\gamma_c+\mu+\tau)(\delta+\gamma_h+\theta+\mu)(\delta+\varepsilon+\gamma_i+\mu)} & \frac{\varepsilon}{(\delta+\gamma_h+\theta+\mu)(\delta+\varepsilon+\gamma_i+\mu)} & \frac{1}{\delta+\gamma_h+\theta+\mu} & 0 \\ \frac{\varepsilon\theta\tau}{(\gamma_c+\mu+\tau)(\delta+\gamma_{ic}+\mu)(\delta+\gamma_h+\theta+\mu)(\delta+\varepsilon+\gamma_i+\mu)} & \frac{\varepsilon\theta}{(\delta+\gamma_{ic}+\mu)(\delta+\gamma_h+\theta+\mu)(\delta+\varepsilon+\gamma_i+\mu)} & \frac{\theta}{(\delta+\gamma_{ic}+\mu)(\delta+\gamma_h+\theta+\mu)} & \frac{1}{\delta+\gamma_{ic}+\mu} \end{pmatrix},$$

Hence, the value of R_0 can be represented by

$$R_0 = R_{0C} + R_{0I} + R_{0H} + R_{0I_c} \tag{10}$$

where,

$$R_{0C} = \frac{(\alpha_2+\mu+(1-\eta)\alpha_1)\beta\rho\phi}{\mu(\alpha_1+\alpha_2+\mu)(\gamma_c+\tau+\mu)}, \tag{11}$$

$$R_{0I} = \frac{(\alpha_2+\mu+(1-\eta)\alpha_1)\beta\tau\phi}{\mu(\alpha_1+\alpha_2+\mu)(\gamma_c+\tau+\mu)(\delta+\varepsilon+\gamma_i+\mu)}, \tag{12}$$

$$R_{0H} = \frac{(\alpha_2+\mu+(1-\eta)\alpha_1)\beta\varepsilon\tau\phi}{\mu(\alpha_1+\alpha_2+\mu)(\gamma_c+\tau+\mu)(\delta+\varepsilon+\gamma_i+\mu)(\delta+\theta+\gamma_h+\mu)}, \tag{13}$$

and

$$R_{0I_c} = \frac{(\alpha_2+\mu+(1-\eta)\alpha_1)\beta\varepsilon\theta\tau\phi}{\mu(\alpha_1+\alpha_2+\mu)(\gamma_c+\tau+\mu)(\delta+\varepsilon+\gamma_i+\mu)(\delta+\theta+\gamma_h+\mu)(\delta+\gamma_{ic}+\mu)}. \tag{14}$$

The complex interactions between several parameters that affect a disease's transmission dynamics are revealed by the basic reproduction number, or R_0. A useful tool for assessing the possible spread of an infection is this epidemiological statistic. Asamoah et al. (2018) optimal is cited. The likelihood of the disease spreading among people is indicated when the R_0 value is higher than 1. In this case, there is a chance of an outbreak because each infected individual often infects multiple new individuals. On the other hand, if the R_0 number is smaller than 1, it indicates that the virus is spreading less quickly over time.

This implies that the disease is not as easily transmissible, and its spread is likely to diminish. The R_0 value is influenced by a range of factors, including: The duration of the infection period, the mode of disease transmission (e.g., direct contact, airborne, contaminated surfaces), the level of population immunity or exposure to the disease, and the frequency of interactions between individuals. Understanding the R_0 value is crucial for formulating effective control strategies and guiding public health interventions. It provides valuable insights into the measures required to mitigate the spread of diseases and safeguard the community. This suggests that the disease is less contagious and that its spread will probably slow down. The length of the infection period, the mode of disease transmission (direct contact, airborne, contaminated surfaces), the degree of population immunity or exposure to the disease, and the frequency of interactions between individuals are some of the factors that affect the R_0 value. Comprehending the R_0 value is essential for developing control measures that work and directing public health initiatives. It offers important information about the steps needed to stop the spread of illnesses and protect the public.

The stability analysis at disease free-equilibrium (DFE)

Now, let's delve into the stability analysis of the equilibrium point (EP). To begin, we introduce the following theorem:

Theorem 4.1 *Let us examine the subsequent system, accompanied by its specified initial conditions*

$$\frac{dX}{dt} = v(t, X(t)), \quad X(t_0) = X_0. \tag{15}$$

*Suppose we make an assumption that the Jacobian matrix, denoted as*15 $J(X^*)$, *is evaluated at an equilibrium point* X^*. *The eigenvalues of J are denoted as* λ_i, *where i ranges from* 1 *to n. In that case, we have the following relationships*:

- X^* *is locally asymptotically stable if* λ_i *satisfies* $|arg(\lambda_i)| > \frac{\pi}{2}$,
- X^* *is unstable if at least one eigenvalue* λ_r *satisfies* $|arg(\lambda_r)| < \frac{\pi}{2}$ *for some* $r \in \{1, 2, \ldots, n\}$.

Moving forward, we denote the Jacobian matrix associated with the equilibrium point representing the absence of disease as:

$$\mathfrak{J} = \begin{pmatrix} -\psi_1 & \alpha_2 & \frac{\beta\rho\psi_2\phi}{\alpha_1\alpha_2 - \psi_1\psi_2} & \frac{\beta\psi_2\phi}{\alpha_1\alpha_2 - \psi_1\psi_2} & \frac{\beta\psi_2\phi}{\alpha_1\alpha_2 - \psi_1\psi_2} & \frac{\beta\psi_2\phi}{\alpha_1\alpha_2 - \psi_1\psi_2} & \sigma \\ \alpha_1 & -\psi_2 & -\frac{\alpha_1\beta(\eta-1)\rho\phi}{\alpha_1\alpha_2 - \psi_1\psi_2} & -\frac{\alpha_1\beta(\eta-1)\phi}{\alpha_1\alpha_2 - \psi_1\psi_2} & -\frac{\alpha_1\beta(\eta-1)\phi}{\alpha_1\alpha_2 - \psi_1\psi_2} & -\frac{\alpha_1\beta(\eta-1)\phi}{\alpha_1\alpha_2 - \psi_1\psi_2} & 0 \\ 0 & 0 & \frac{\alpha_1(\beta(\eta-1)\rho\phi - \alpha_2\psi_3) + \psi_2(\psi_1\psi_3 - \beta\rho\phi)}{\alpha_1\alpha_2 - \psi_1\psi_2} & \frac{\beta\phi(\alpha_1(\eta-1) - \psi_2)}{\alpha_1\alpha_2 - \psi_1\psi_2} & \frac{\beta\phi(\alpha_1(\eta-1) - \psi_2)}{\alpha_1\alpha_2 - \psi_1\psi_2} & \frac{\beta\phi(\alpha_1(\eta-1) - \psi_2)}{\alpha_1\alpha_2 - \psi_1\psi_2} & 0 \\ 0 & 0 & \tau & -\psi_4 & 0 & 0 & 0 \\ 0 & 0 & 0 & \varepsilon & -\psi_5 & 0 & 0 \\ 0 & 0 & 0 & 0 & \theta & -\psi_6 & 0 \\ 0 & 0 & \gamma_c & \gamma_i & \gamma_h & \gamma_{ic} & -\sigma \end{pmatrix}, \tag{16}$$

where

$$\begin{cases} \psi_1 = \alpha_1 + \mu, \\ \psi_2 = \alpha_2 + \mu, \\ \psi_3 = \gamma_c + \mu + \tau, \\ \psi_4 = \delta + \varepsilon + \gamma_i + \mu, \\ \psi_5 = \delta + \gamma_h + \theta + \mu, \\ \psi_6 = \delta + \gamma_{ic} + \mu. \end{cases} \tag{17}$$

The eigenvalues of the Jacobian matrix $\mathfrak{J}$ are

Table 2 Description of model system 1 parameters

Parameter	Value	Source
ϕ	7.27892×10^{1}	Estimated
α_1	0.001	Fixed
α_2	0.169	Fixed
β	2.83562×10^{-5}	Fitted
η	0.145362	Fitted
γ_c	0.0438	Fitted
τ	0.0427	Fitted
ε	0.036246	Fitted
γ_i	0.062365	Fitted
γ_h	0.003336	Fixed
γ_{ic}	0.002376	Fitted
σ	0.001236	Fitted
ρ	0.00242	Fitted
μ	$\frac{1}{(57.6\times365)}$	Estimated
δ	0.0454	Fitted
δ	0.123	Fitted

$$\begin{cases} \lambda_1 = -\mu < 0, \\ \lambda_2 = -\sigma < 0, \\ \lambda_3 = -\alpha_1 - \alpha_2 - \mu < 0. \end{cases} \tag{18}$$

The remaining eigenvalues is analysed by using the polynomial

$$\lambda^3 + a_1\lambda^2 + a_2\lambda + a_3 = 0, \tag{19}$$

where a_1, a_2, a_3, are quite difficult to write; as a result, we have left their values out. The polynomial (19) with real coefficients satisfies the requirement that all of its roots are either negative or have negative real parts in accordance with the Routh–Hurwitz criteria if and only if $a_1 > 0, a_3 > 0, a_2a_1 > a_3$ which implies $a_2 > 0$ and the corresponding Hurwitz matrices $H_1, H_2,$, and H_3 have ono-negativedeterminants. i.e.,

$$|H_i| > 0 \quad \text{for} \quad i = 1, 2, 3, \tag{20}$$

where

$$H_1 = (a_1), H_2 = \begin{pmatrix} a_1 & 1 \\ a_3 & a_2 \end{pmatrix}, H_3 = \begin{pmatrix} a_1 & 1 & 0 \\ a_3 & a_2 & a_1 \\ 0 & 0 & a_3 \end{pmatrix}. \tag{21}$$

Therefore, if (20) is met, the disease-free equilibrium point is locally asymptomatically stable.

Our next goal is to identify the disease-free equilibrium point's zones of stability and instability. While stability regions will be displayed in a distinct color, instability regions will be indicated in yellow. With Table 2's preset parameter values in mind, we can determine the stability regions for the disease-free equilibrium point in various parameter planes, as illustrated in Figs. 3, 4 and 5. The analysis of Fig. 3 reveals an intriguing pattern - as the vaccination rate (α_1) increases, the stability region for the disease-free equilibrium point also expands. This

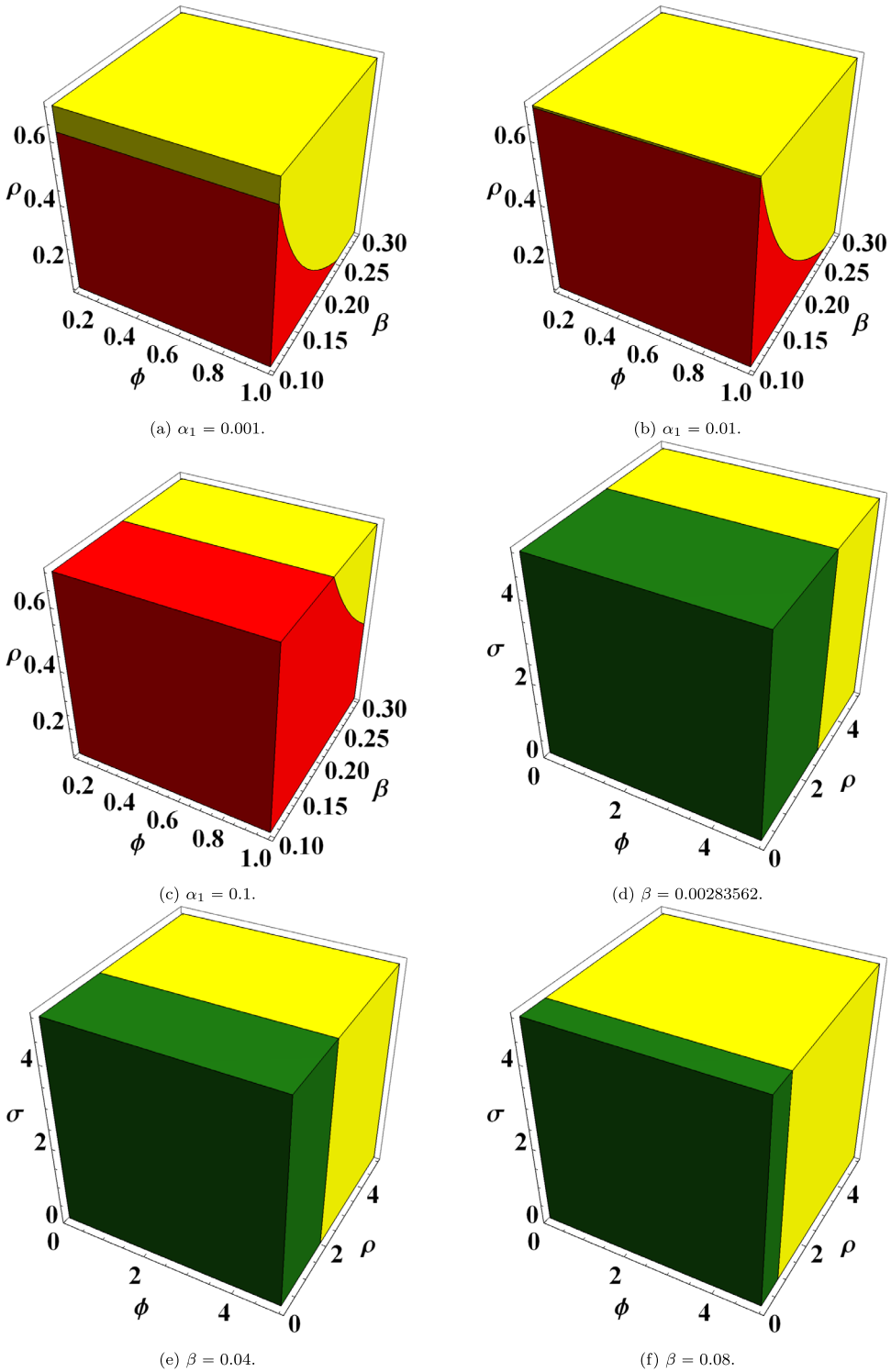

Fig. 3 3D stability and instability of parameters for the disease-free equilibrium point: $\phi - \beta - \rho$, and $\phi - \rho - \sigma$ regions

relationship is clearly demonstrated through the three subfigures presented. In Fig. 3a, the vaccination rate α_1 is set to a relatively low value of 0.001. This corresponds to a smaller stability region for the disease-free equilibrium. On the other hand, when α_1 is increased to 0.01 in Fig. 3b, the stability region is observed to grow in size. Finally, when the vaccination rate is further elevated to 0.1 in Fig. 3c, the stability region expands even more, occupying a larger portion of the parameter space. This pattern highlights the important role that the vaccination rate plays in determining the stability characteristics of the disease-free equilibrium point within the system under investigation. When the

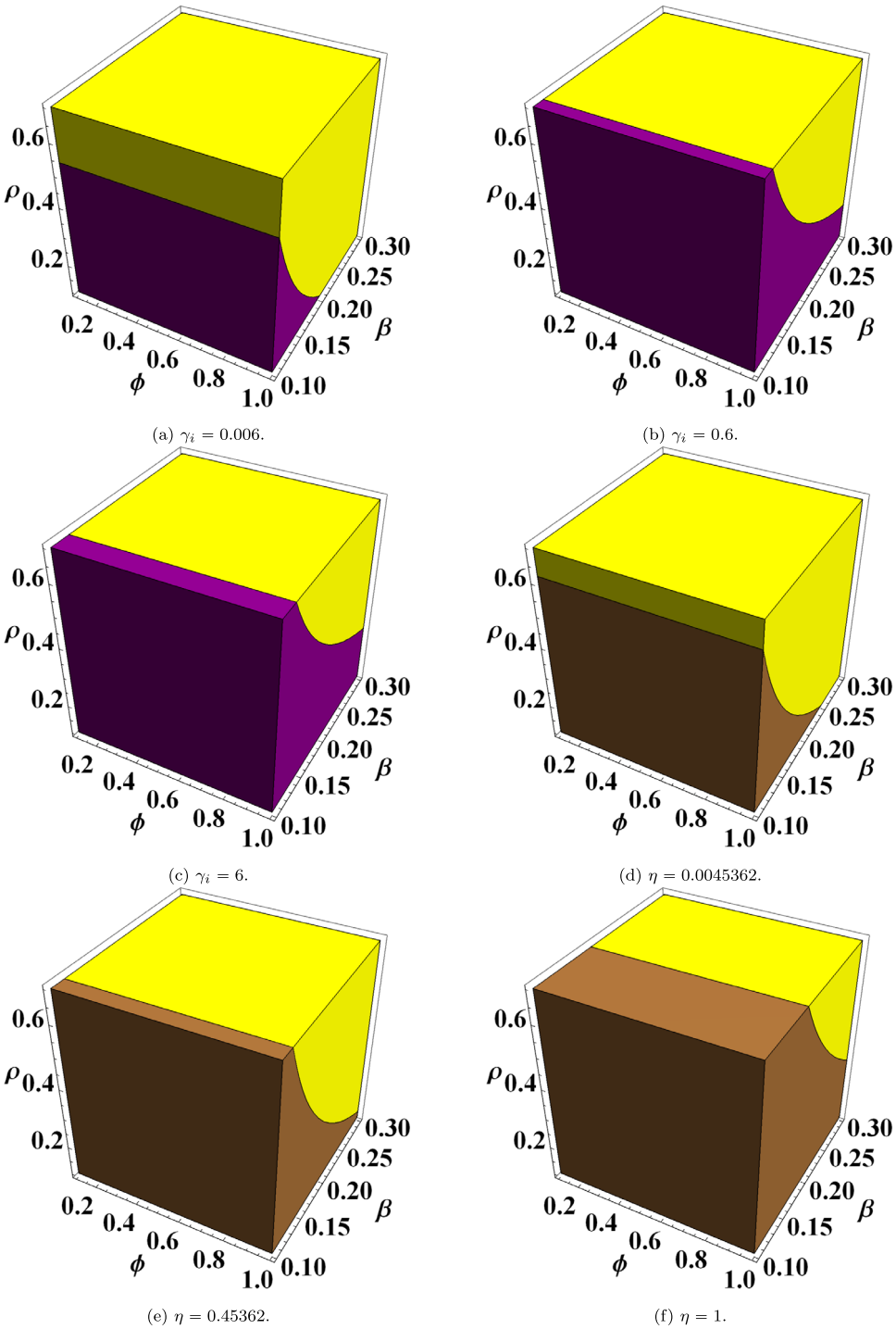

(a) $\gamma_i = 0.006$. (b) $\gamma_i = 0.6$.

(c) $\gamma_i = 6$. (d) $\eta = 0.0045362$.

(e) $\eta = 0.45362$. (f) $\eta = 1$.

Fig. 4 3D stability and instability regions of parameters for the disease-free equilibrium point: $\phi - \beta - \rho$ region

effective contact rate (β) increases, the stability region for the disease-free equilibrium point shrinks. Also, this relationship is clearly demonstrated through the three subfigures presented. In Fig. 3d, effective contact rate β is set to a relatively low value of 0.00283562. This corresponds to a larger stability region for the disease-free equilibrium. On the other hand, when β is increased to 0.04 in Fig. 3e, the stability region is observed to reduce in size. Finally, when the effective contact rate is further elevated to 0.08 in Fig. 3f, the stability region shrinks even more, occupying a smaller portion of the parameter space. The analysis of Fig. 4 reveals that as the recovery rate from symptomatic infected class (γ_i) increases, the stability region for the disease-free equilibrium point also expands. This relationship is clearly demonstrated through the three subfigures presented. In Fig. 4a, the vaccination rate γ_i is set to a

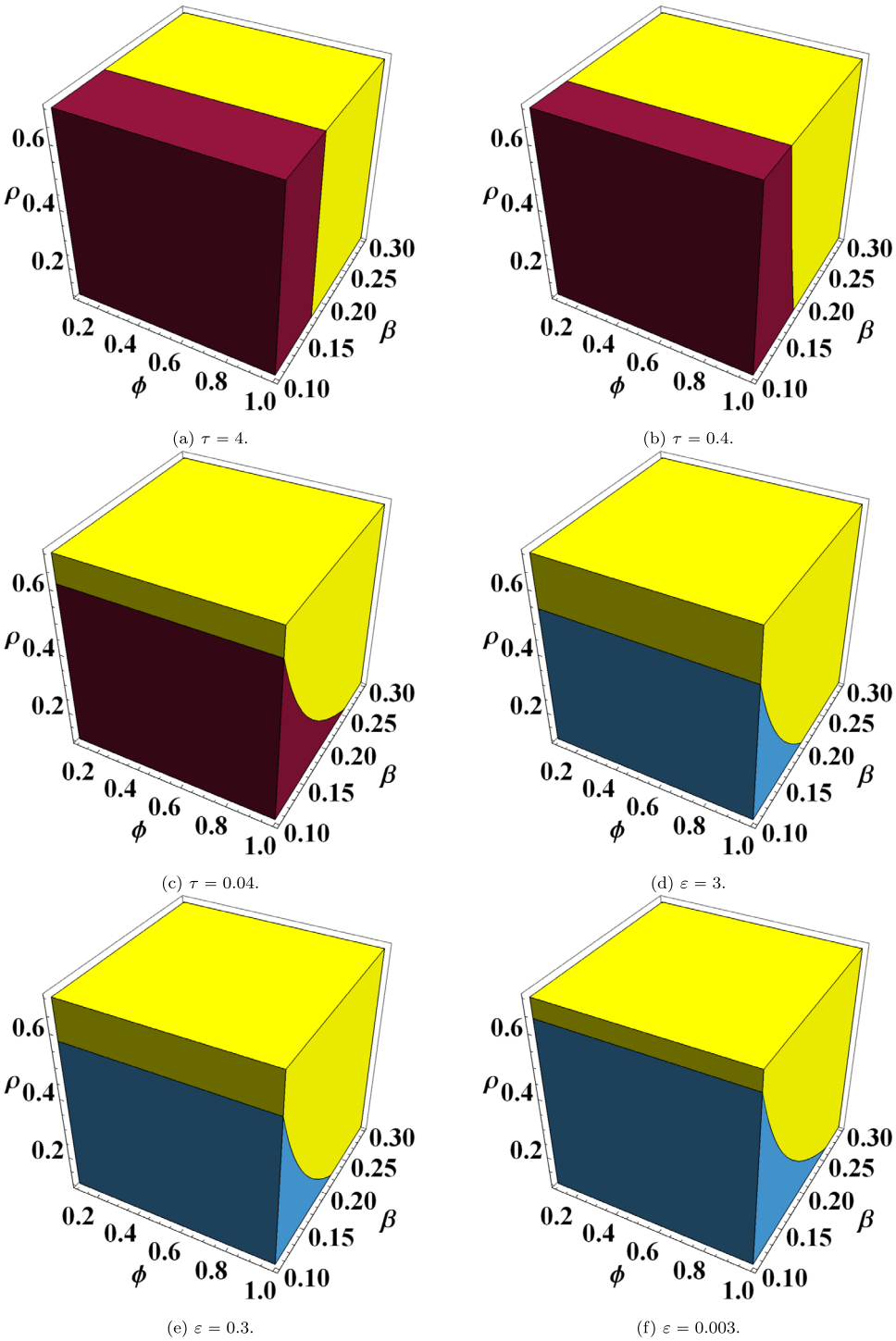

(a) $\tau = 4$. (b) $\tau = 0.4$.

(c) $\tau = 0.04$. (d) $\varepsilon = 3$.

(e) $\varepsilon = 0.3$. (f) $\varepsilon = 0.003$.

Fig. 5 3D stability and instability regions of parameters for the disease-free equilibrium point: $\phi - \beta - \rho$ region

relatively low value of 0.006. This corresponds to a smaller stability region for the disease-free equilibrium. On the other hand, when γ_i is increased to 0.6 in Fig. 4b, the stability region is observed to grow in size. When the vaccination rate is further elevated to 6 as presented in Fig. 4c, the stability region expands even more, occupying a larger portion of the parameter space. The analysis of Fig. 4 reveals that as the vaccine efficacy (η) increases, the stability region for the disease-free equilibrium point also expands. This relationship is clearly demonstrated through the three subfigures presented. In Fig. 4d, the vaccine efficacy η is set to a relatively low value of 0.0045362. This corresponds to a smaller stability region for the disease-free equilibrium. On the other hand, when η is increased to 0.45362 in Fig. 4e, the stability region is observed to grow in size. Finally, when the vaccine efficacy is further

elevated to 1 in Fig. 4f, the stability region expands even more, occupying a larger portion of the parameter space. In Fig. 5, when rate of progression from carrier class to symptomatic infected class (τ) decreases, the stability region for the disease-free equilibrium point shrinks. Also, this relationship is clearly demonstrated through the three subfigures presented. In Fig. 5a, τ is set to a relatively large value of 4. This corresponds to a larger stability region for the disease-free equilibrium. On the other hand, when τ is decreased to 0.4 in Fig. 5b, the stability region is observed to reduce in size. Finally, when τ is further decreased to 0.04 in Fig. 5c, the stability region shrinks even more, occupying a smaller portion of the parameter space. When the rate of progression from symptomatic infected class to hospitalization (ε) decreases, the stability region for the disease-free equilibrium point increases. Also, this relationship is clearly demonstrated through the three subfigures presented. In Fig. 5d, ε is set to a relatively large value of 3. This corresponds to a smaller stability region for the disease-free equilibrium. On the other hand, when ε is decreased to 0.3 in Fig. 5e, the stability region is observed to increase in size. Finally, when ε is decreased to 0.003 in Fig. 5f, the stability region expands even more, occupying a larger portion of the parameter space.

Sensitivity index

The calculation of the basic reproduction number, R_0, indicates that it is influenced by all the parameters presented in Table 2, with the exception of σ and γ_c. In this subsection, we will explore how the spread of the disease is affected by these remaining parameters. The parameter space under consideration is defined as follows:

$$\Omega := \{(\phi, \beta, \rho, \alpha_1, \alpha_2, \mu, \eta, \tau, \delta, \varepsilon, \gamma_i, \theta, \gamma_h, \gamma_{ic}) \in \mathbb{R}^{+}_{14}\}. \tag{22}$$

The following definition is proposed by Chitnis et al. (2008):

Definition 4.2 (Chitnis et al. 2008) The sensitivity index of R_0 with respect to a parameter p, which is a member of $C^1(\Omega)$, is defined as follows:

$$\sum_{p}^{R_0} = \frac{\partial R_0}{\partial p} \times \frac{p}{R_0}. \tag{23}$$

The normalized relative change in R_0 that results from changing one parameter while holding the others constant is computed using this definition. Each parameter's sensitivity index is frequently defined by intricate analytical formulations that hardly ever offer insightful data or insights. When the sensitivity index is positive, it means that R_0 rises with the parameter; when it is negative, it means that R_0 falls with the parameter.

We now present some examples. Based on the previous form of R_0, we obtain the following (see Fig. 6):

$$\sum_{\delta}^{R_0} = \left[\frac{\frac{\partial R_0}{R_0}}{\frac{\partial \delta}{\delta}}\right] = -\frac{\alpha_1 \eta}{\alpha_1(1-\eta)+\alpha_2+\mu},$$

$$\sum_{\phi}^{R_0} = \left[\frac{\frac{\partial R_0}{R_0}}{\frac{\partial \phi}{\phi}}\right] = 1,$$

$$\sum_{\beta}^{R_0} = \left[\frac{\frac{\partial R_0}{R_0}}{\frac{\partial \beta}{\gamma_1}}\right] = 1.$$

The long-term success in managing an epidemic situation greatly relies on the efficient implementation of

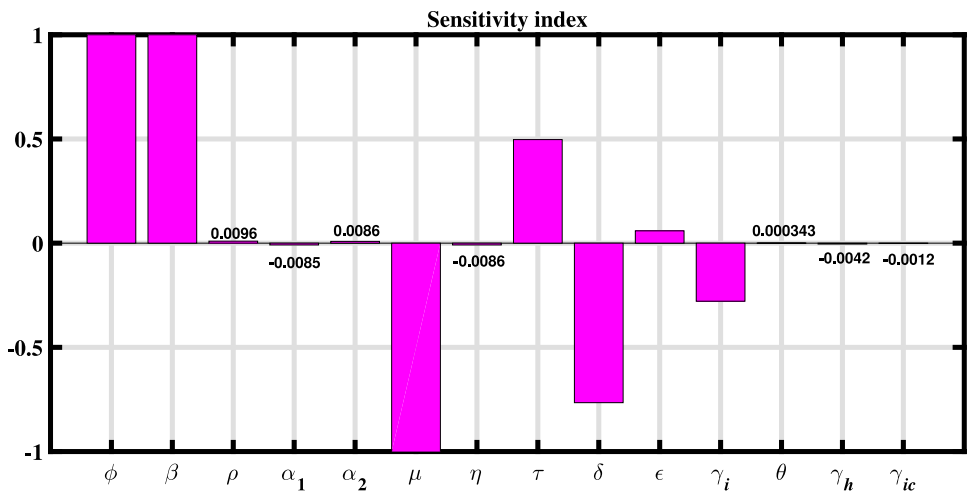

Fig. 6 The sensitivity index of R_0 to various parameters in model (1)

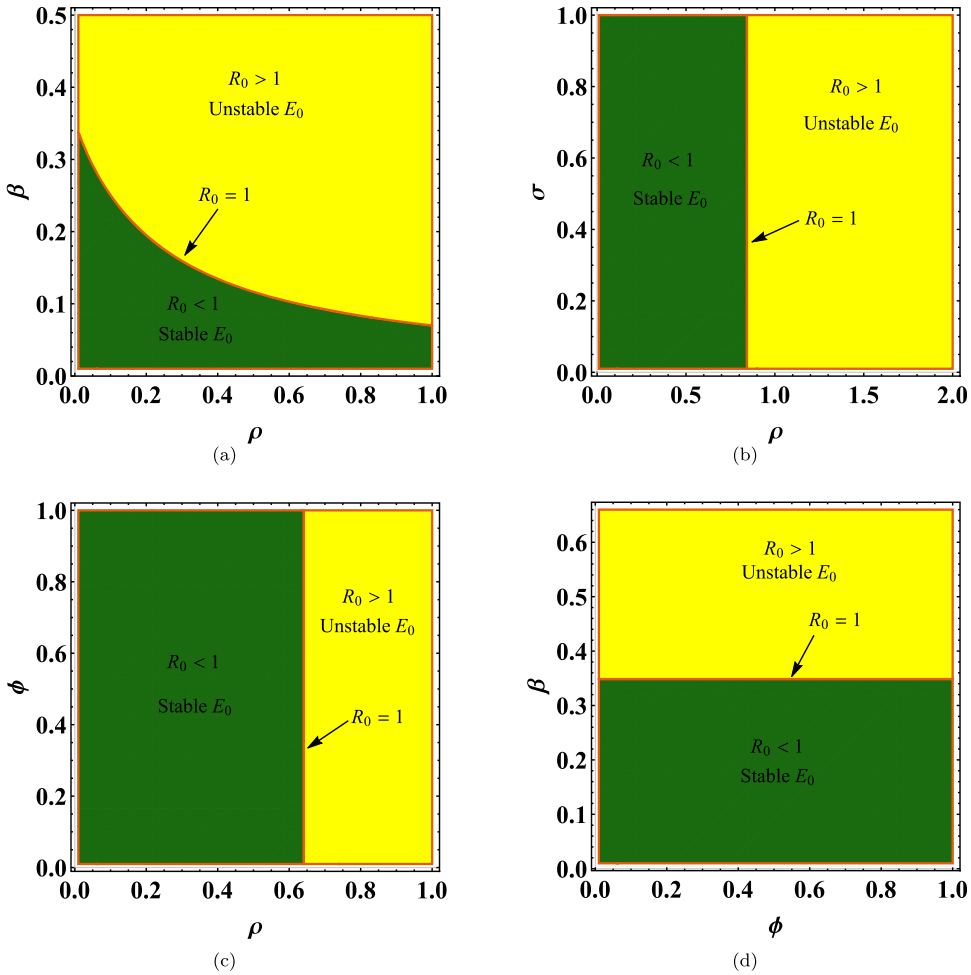

Fig. 7 Some stability and instability regions of parameters for the disease-free equilibrium point with different values of R_0

government measures and the strict adherence to regulations. When a disease outbreak occurs, it is of utmost importance for the general public to willingly embrace essential behavioral changes in order to disrupt the transmission chain. On the other hand, if the disease rapidly spreads among the population, controlling it becomes increasingly challenging and necessitates a prompt and decisive response. The management of an epidemic crisis relies significantly on the public's response. By raising public awareness and providing education, we can effectively halt the spread of diseases. This enables individuals to take necessary precautions and become well-informed about preventive measures. Additionally, the recovery of affected individuals, whether through therapeutic intervention or the development of natural immunity, plays a crucial role in reducing the overall prevalence of the disease. Individuals who have recovered from an illness are at a reduced risk of spreading the disease, thereby alleviating the burden on the healthcare system. Furthermore, a decrease in the reproduction number indicates a decline in disease transmission due to fewer individuals being sick. This underscores the significance of boosting the immunization rate against the infection. To effectively curb the spread of the infection, it is crucial for the vaccine to be highly effective, particularly in providing a high level of protection.

Figure 7 illustrates the regions of stability and instability for parameters associated with disease-free EPs at various values of R_0. The green regions on the graph represent stability, indicating that R_0 is below one. On the other hand, the yellow regions indicate instability, with R_0 exceeding one.

Data fitting and numerical simulation

Understanding disease epidemics requires the use of mathematical modeling. By successfully reproducing observed incidence and prevalence statistics, researchers have gained important insights into the course of disease and effective management measures. We can develop precise forecasts regarding upcoming outbreaks and measure the degree of uncertainty in these forecasts by verifying these models using actual data. In this part, we

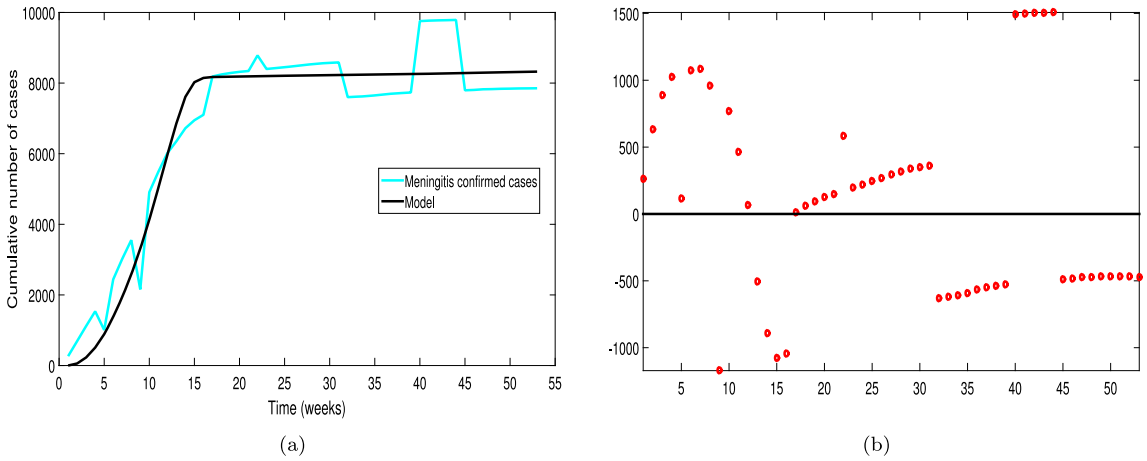

Fig. 8 Real statistics cases in Nigeria and the associated **b** residual plot show the best fit of the proposed meningitis model

describe the dynamics of the meningitis outbreak by fitting our suggested model to actual data from Nigeria.

The Nigerian Centre for Disease Control (NCDC) database provided us with information on meningitis cases that were reported in Nigeria during the first week of January and the final week of December 2023 (NCDC 2019). Weekly counts of cases and fatalities are included in these data, and they form the foundation for model fitting and parameter estimation. For our model to be dependable, precise parameter estimation is essential. To find the model parameters, we used a combination of data fitting and parameter estimation techniques.

The median lifespan of Nigeria, which is 60.87 years, was used to compute the natural death rate of humans. The natural death rate, which is the percentage of the population that passes away from natural causes each week, is $\frac{1}{60.87\times 53}$ per week when converted to a weekly rate. With N stated as 219,463,862 (NCDC 2019), the recruitment rate ($\mu \times N$) is the rate at which new people are added to the population. The ratio of the total number of reported deaths to the total number of cases reported during the study period was used to calculate the meningitis mortality rate (δ): $\delta = \frac{\sum_{t=1}^{n} D_t}{\sum_{t=1}^{n} I_t}$, where $t = 1, 2, \ldots, n$ represents each week in the 53-week period. Given a meningitis infection, this parameter shows the likelihood of death. We fitted the cumulative confirmed reported cases to our meningitis model using the conventional nonlinear least squares method, modifying the model parameters until the predicted values roughly matched the actual data, to make sure our model accurately reflects the real-world data. Table 2 provides a summary of the estimated and fitted parameter values. Figure 8a illustrates the data fitting procedure, displaying the observed cumulative cases in addition to the model's predictions. Figure 8b shows the residuals. We can gain a better understanding of the dynamics of the meningitis outbreak among the population by fitting our suggested model to actual data from Nigeria. Our forecasts are based on real data according to the parameter estimation and model fitting processes, which increases their dependability for public health planning and intervention tactics. This thorough method shows how effective mathematical modeling can be when dealing with difficult epidemiological problems.

Numerical simulations and discussion of results

In this section, we discuss the dynamics of meningitis in the human population by considering the parameters that drive its transmission. We use estimated and fitted parameters that are summarized in Table 2.

Effect of contact rate on meningitis transmission dynamics

This subsection focuses on investigating the impact of the effective contact rate, β on different population classes. The results from numerical simulations are presented in Fig. 9a to Fig. 9g. Understanding the dynamics of infectious disease propagation requires an understanding of how the contact rate β affects different compartments of a disease model. The effects of varying levels of β on the susceptible (S), vaccinated (V), carrier (C), infected (I), hospitalized (H), intensive care (I_c), and recovered (R) populations are depicted in Figs. 9a through 9g. Due to increased exposure to the virus, Fig. 9a shows that as β increases, the susceptible population falls more quickly, especially at $\beta = 5 \times 10^{-5}$. A similar tendency can be seen in Fig. 9b for the group that received vaccinations, where higher β results in a more significant reduction because of

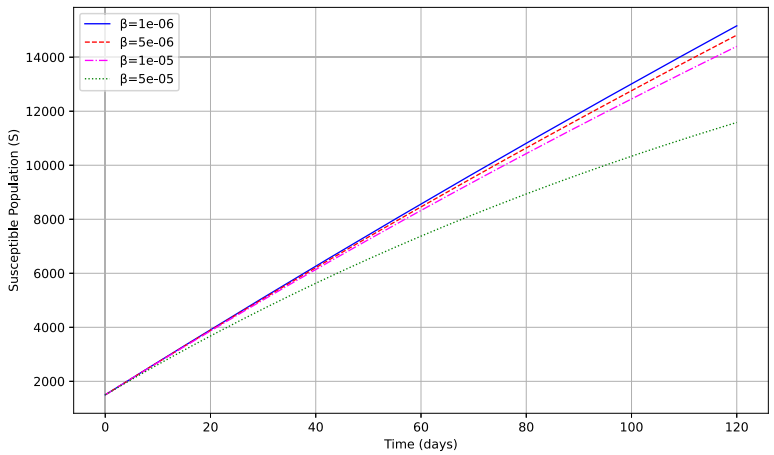

(a)

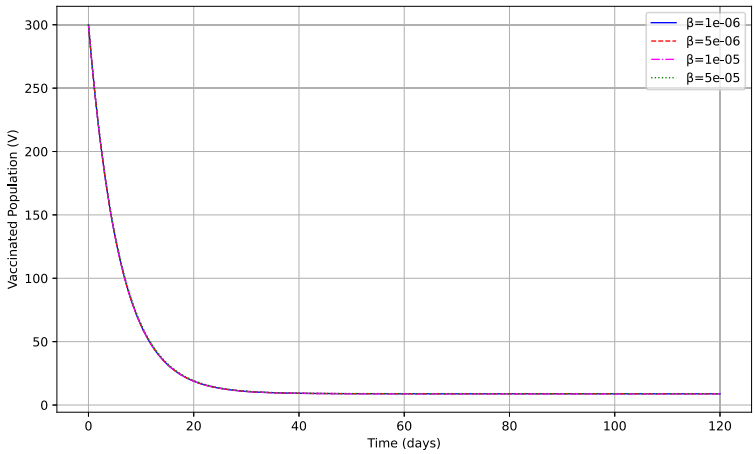

(b)

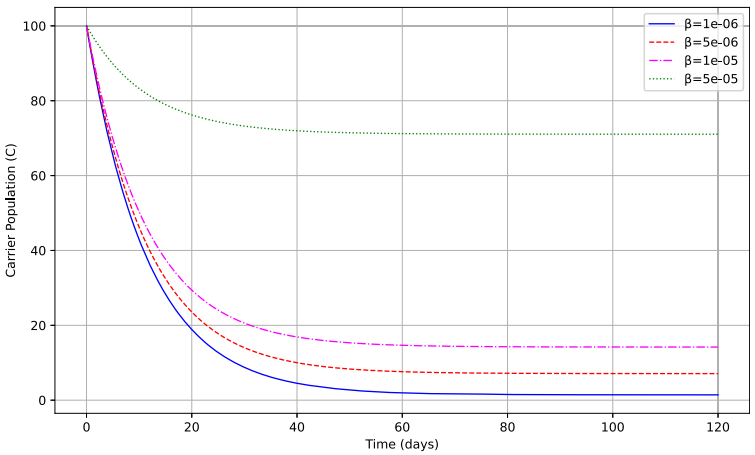

(c)

Fig. 9 Effect of contact Rate on meningitis transmission dynamics

Fig. 9 continued

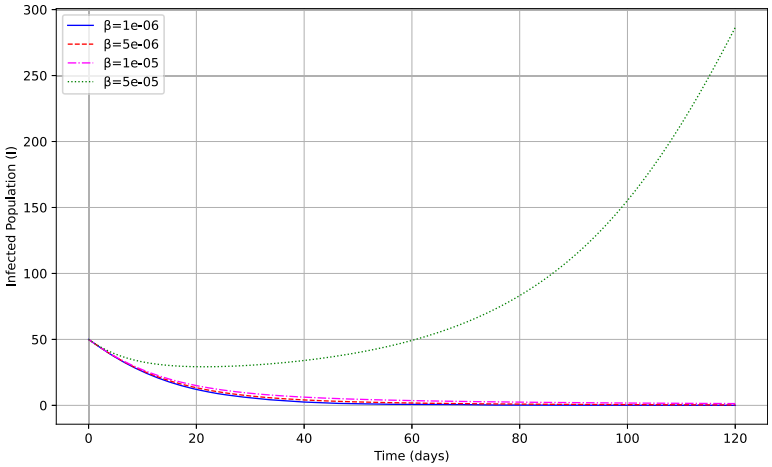

(d)

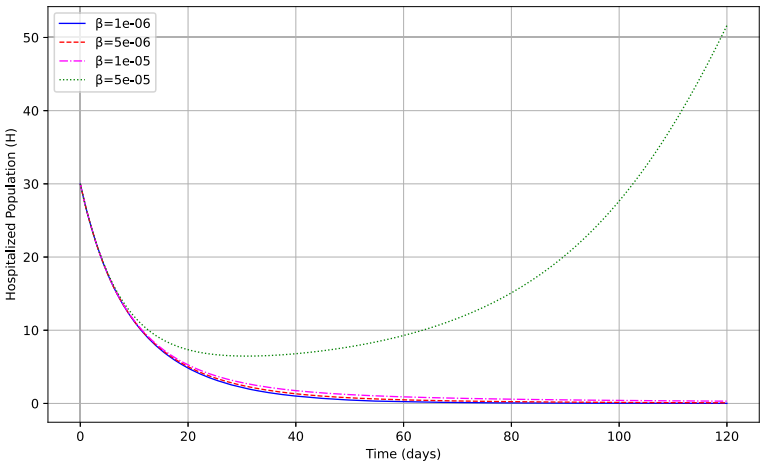

(e)

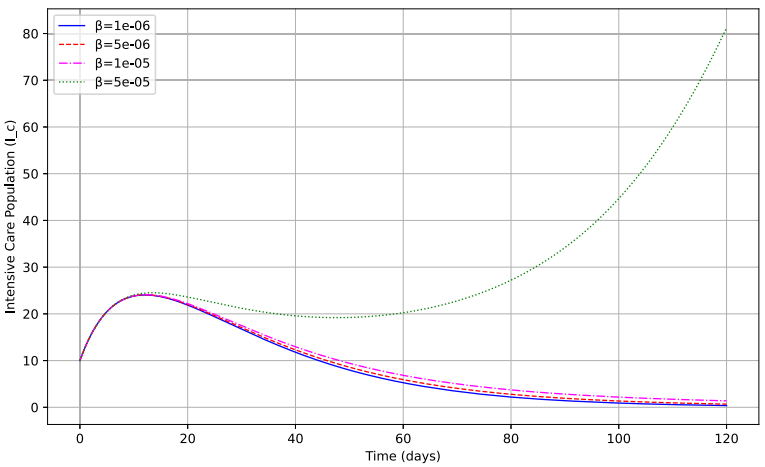

(f)

Fig. 9 continued

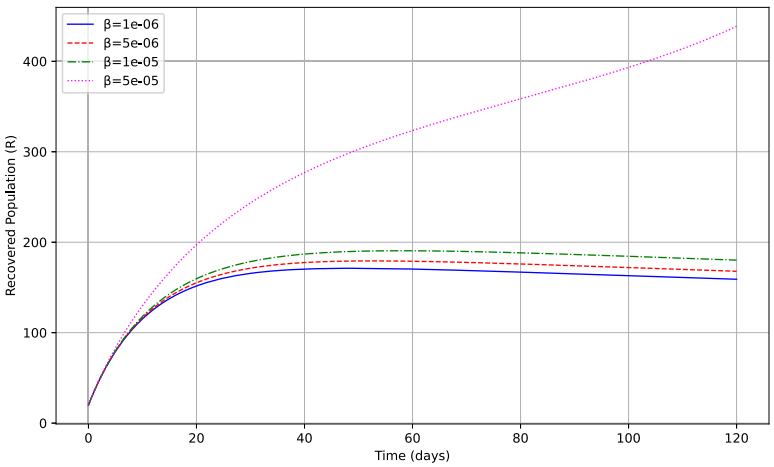

(g)

increased exposure even after initial immunity. As more people reach the carrier state, Fig. 9c shows that the carrier population increases rapidly with greater β, particularly at $\beta = 5 \times 10^{-5}$. As seen in Fig. 9d, the infected population rises drastically with β, again increasing at $\beta = 5 \times 10^{-5}$ at the fastest rate. Figure 9e illustrates how the number of hospitalized patients rises with an increase in β, suggesting a greater strain on healthcare systems, especially at $\beta = 5 \times 10^{-5}$. In a similar vein, Fig. 9f emphasizes that the population in critical care increases sharply as β rises, highlighting the risk of overcrowding medical facilities. Lastly, Fig. 9g shows that as β increases, so does the recovered population, with the maximum recovery rate occurring at $\beta = 5 \times 10^{-5}$. Together, these figures highlight the critical role that controlling the contact rate β plays in limiting the transmission and effect of infectious diseases.

Effect of vaccination on meningitis transmission dynamics

This subsection aims to present and discuss the effect of vaccination on each sub-population. Numerical simulation results are shown in Fig. 10.

The findings displayed in Fig. 10a–g show how varying vaccination rates, indicated by α_1, affect distinct demographic subgroups. The susceptible population in Fig. 10a falls more dramatically with increasing vaccination rate α_1; the largest reduction occurs at $\alpha_1 = 0.18$. This is to be expected as fewer people are at risk of infection when vaccination rates are greater. The vaccinated population increases highest when $\alpha_1 = 0.18$, as Fig. 10b illustrates. This suggests that more people are receiving vaccinations at this pace. Although the dynamics of the outbreak vary, Fig. 10c's carrier population illustrates how all scenarios eventually converge and subsequently decline, indicating that even though the overall number of cases initially rises, the outbreak is ultimately contained across all vaccination rates. As seen in Fig. 10d, the lower percentage of vaccinated people causes the infected population to expand more at $\alpha_1 = 0.1$, which facilitates the infection's wider spread. The hospitalized population in Fig. 10e exhibits a greater increase at $\alpha_1 = 0.1$, indicating that reduced vaccination rates cause more infections and, in turn, more severe cases that need to be hospitalized. Similar trends to hospitalizations are seen in Fig. 10f, which shows the population of intensive care units. Lower vaccination rates correspond to a higher number of patients in critical care. Lastly, Fig. 10g illustrates how, as more individuals contract an infection and then recover, the recovered population grows higher at $\alpha_1 = 0.1$. Overall, the findings demonstrate how more vaccinations can effectively lower the susceptible and infected populations thereby controlling the spread of the disease and preventing hospital overload.

Figure 10 illustrates the variations in each sub-population as the vaccination rate changes. Notably, the figure shows that susceptible and vaccinated individuals increases with an increase in vaccination rate, while carriers, infectious, hospitalized and people at intensive care decreases with an increase in vaccination rate. This implies that vaccination reduces infection rate as immunised individuals will be introduced in the population. Additionally, it can be observed that each sub-population decreases over time.

Effect of carriers on meningitis transmission dynamics

In this subsection presents the contribution of asymptomatic individuals;infected individuals with no disease

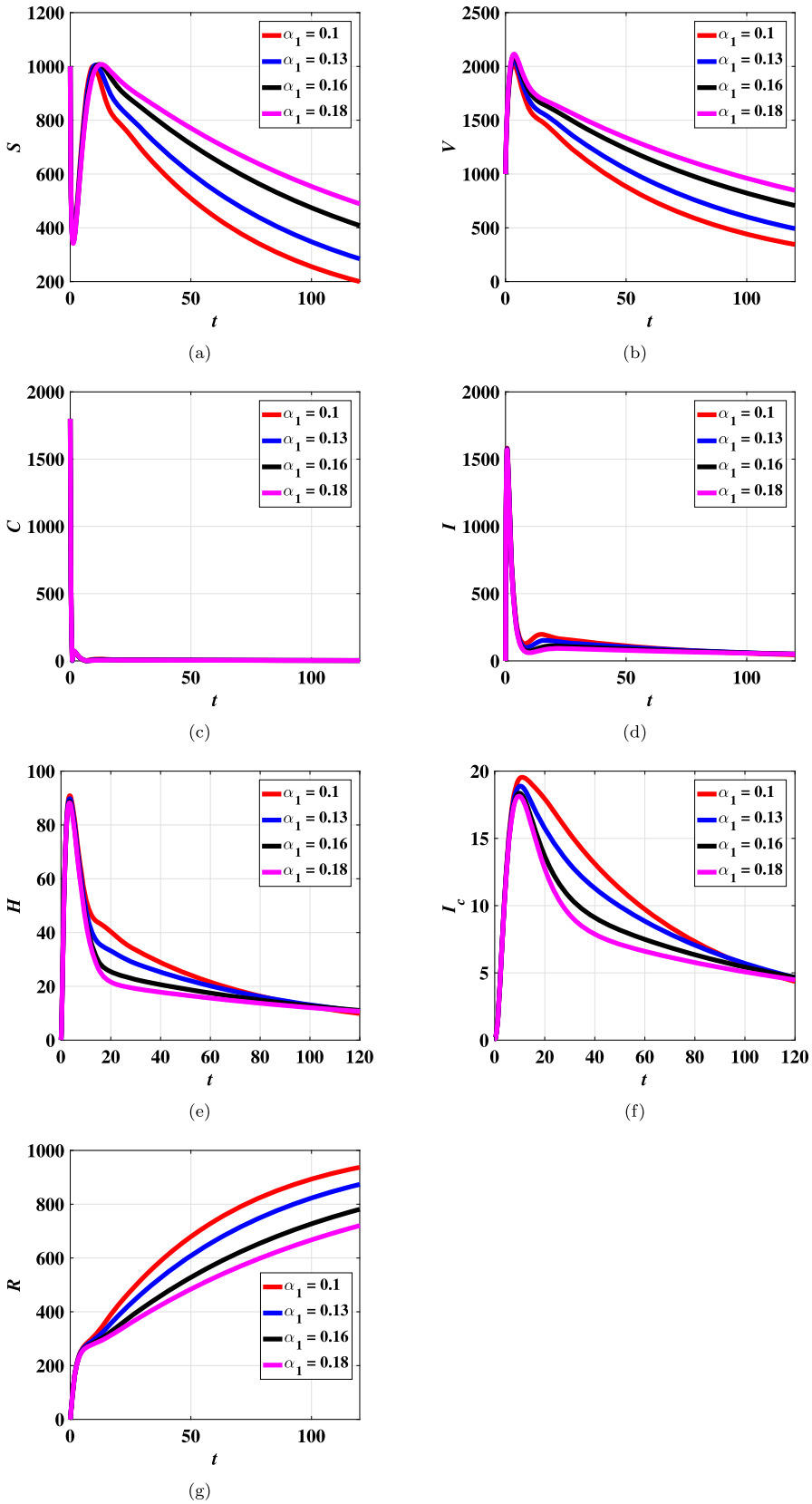

Fig. 10 Dynamical behavior state variables for endemic case when α_1 is varied

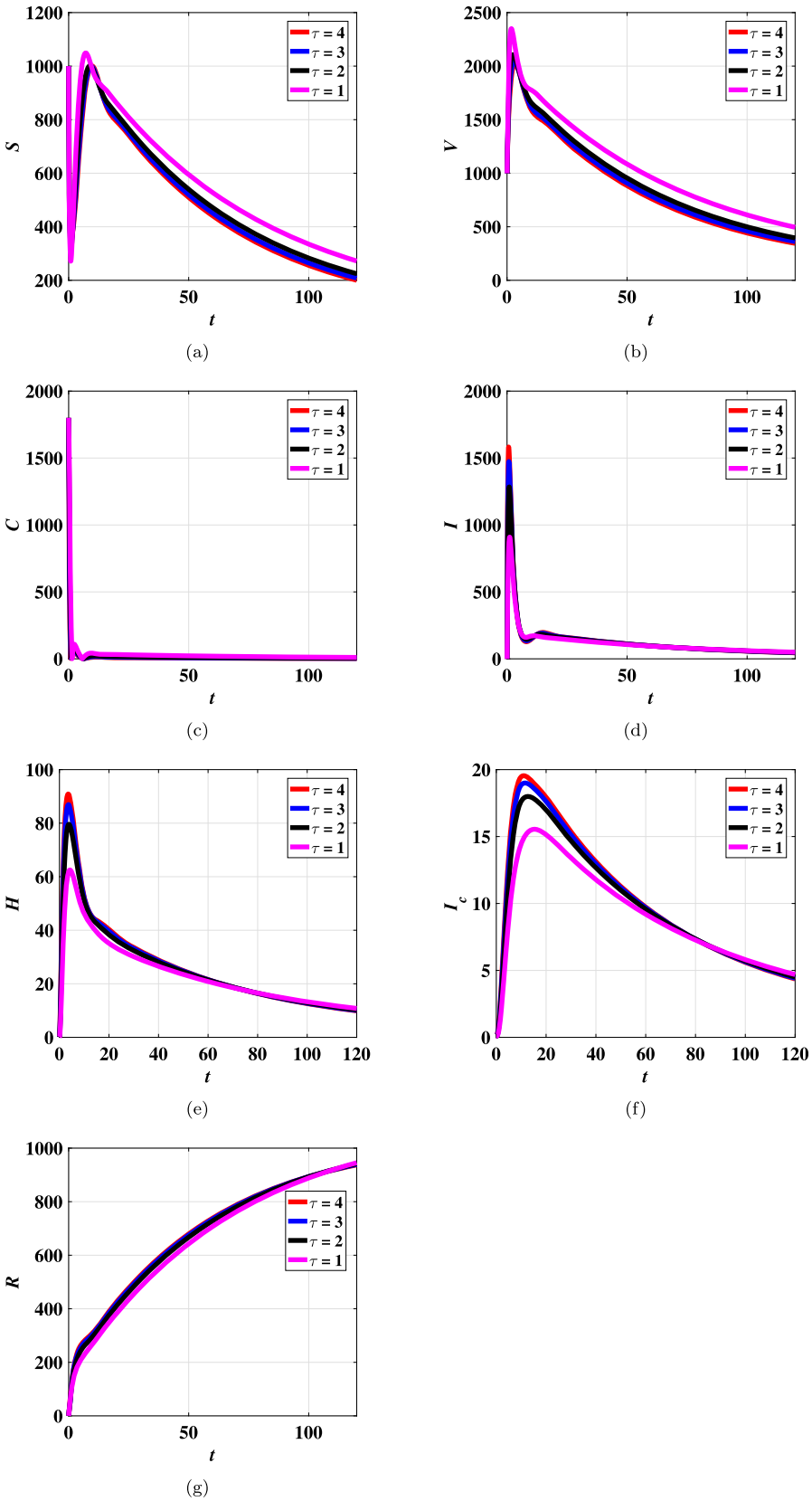

Fig. 11 Dynamical behavior state variables for endemic case when τ is varied

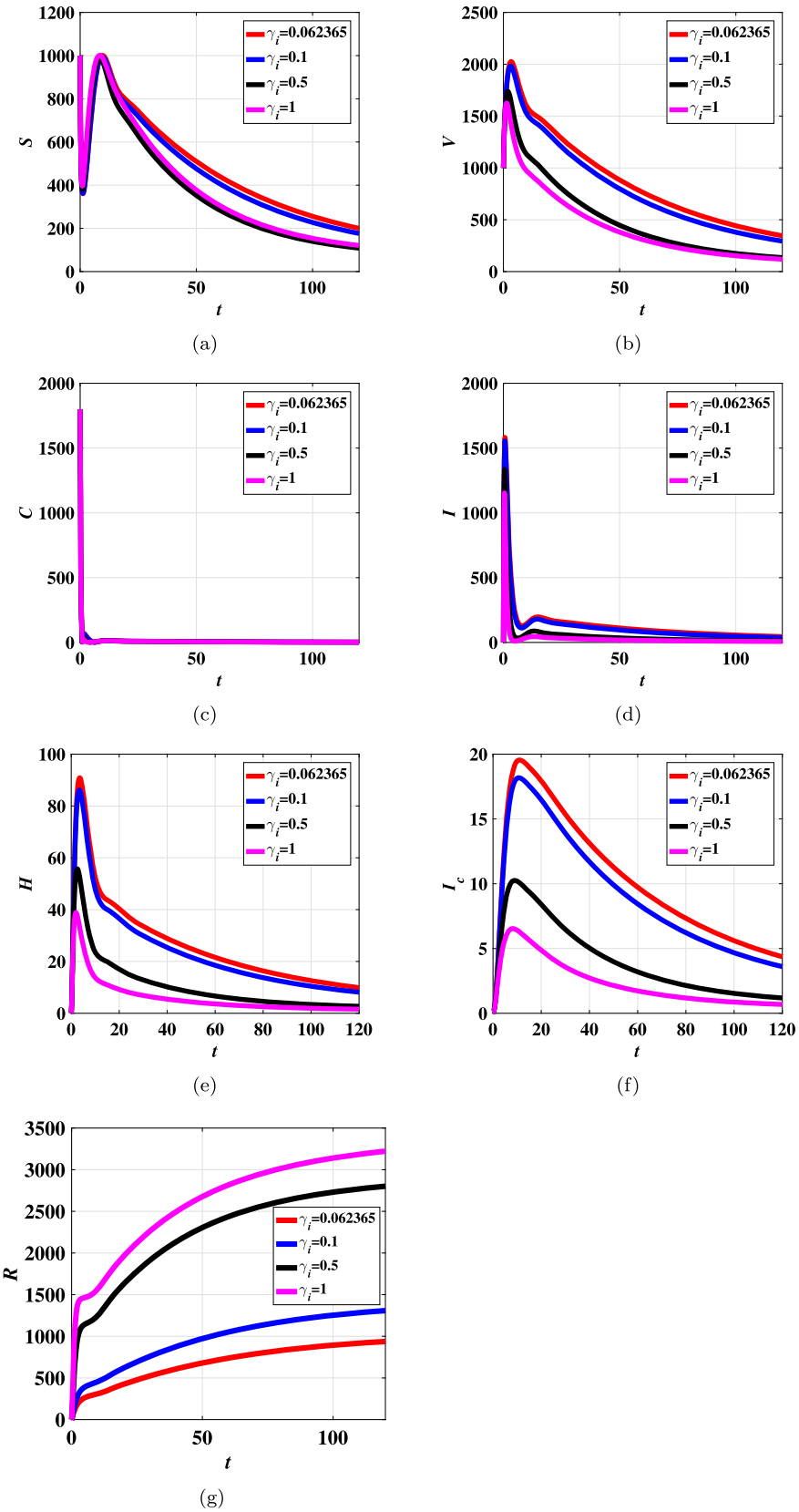

Fig. 12 Dynamical behavior of state variables for endemic case when γ_i is varied

symptoms on the transmission dynamics of meningitis disease. Figure 11 illustrates the findings.

Furthermore, Fig. 11 shows the changes in each sub-population as the rate of progression from asymptomatic to symptomatic classes varies. The figure clearly demonstrates that as the progression rate increases, each sub-population decreases. Additionally, it can be observed that all sub-populations decline over time. This is because symptomatic individuals, being aware of their disease status, may take deliberate actions to protect others in the community. Moreover, individuals exhibiting symptoms alert others to take precautions, effectively blocking many potential transmission routes.

On the other hand, Fig. 12g indicates that an increase in the number of vaccinated and hospitalized individuals, as well as those under intensive care, leads to a higher recovery rate. Additionally, the number of carriers and infectious individuals decreases as the recovery rate increases.

Conclusion

The development and evaluation of a mathematical model for the dynamics and control of meningitis transmission was the main goal of this work. To improve disease management strategies and have an impact on public health policy, it specifically provided a thorough investigation of the epidemiological patterns of meningitis in Nigeria. The Next Generation Matrix operator approach was used to calculate the basic reproduction number, which was then used to determine the prerequisites for the stability and presence of the equilibrium points.

It was discovered that if $R_0 < 1$ and $R_0 > 1$, respectively, then there are meningitis-free and meningitis-persistent equilibria that are stable both locally and globally. The most sensitive metrics that should be the focus of intervention methods are the rates of recruitment, effective contact, progression from carrier to symptomatic, and disease-induced death, according to sensitivity analysis.

Furthermore, results from numerical simulations and analytical solutions show that while vaccination is a successful control measure, additional work is needed to reduce contact between vulnerable and infected people. We think our model can give public health officials important information to forecast the consequences of meningitis transmission, examine its underlying causes, and direct future control initiatives. Future research can examine how public health education, screening, and treatment of asymptomatic infected persons affect the disease's transmission and management. Furthermore, cost-effectiveness and optimal control assessments of the control strategies may be worthwhile study topics in the future.

Below are the key findings from the study

- Critical parameters influencing meningitis transmission include recruitment rates, effective contact, disease progression, and mortality.
- Vaccination is effective but requires complementary strategies to reduce contact between susceptible and infected individuals.
- The model aids in predicting outbreaks and guiding public health interventions.
- Recommendations for future research include public health education, screening of asymptomatic carriers, and cost-effective control strategies.

Funding No funding received

Data Availability The article contains the data that validated the study's conclusions. The Nigerian Center for Disease Control data set, which is displayed in Table 2, was used by the authors to estimate a set of parameter values.

Declarations

Conflict of interest None to declare.

References

Abioye AI, Ibrahim MO, Peter OJ, Ogunseye HA (2020) Optimal control on a mathematical model of malaria. Sci Bull Ser A Appl Math Phys 82(3):177–190

Abioye AI, Peter OJ, Ogunseye HA, Oguntolu FA, Oshinubi K, Ibrahim AA, Khan I (2021) Mathematical model of covid-19 in Nigeria with optimal control. Results Phys 28:104598

Abioye AI, Peter OJ, Addai E, Oguntolu FA, Ayoola TA (2024) Modeling the impact of control strategies on malaria and covid-19 coinfection: insights and implications for integrated public health interventions. Qual Quant 58(4):3475–3495

Asamoah JKK, Nyabadza F, Seidu B, Chand M, Dutta H (2018) Mathematical modelling of bacterial meningitis transmission dynamics with control measures. Comput Math Methods Med 2018(1):2657461

Asamoah JKK, Nyabadza F, Jin Z, Bonyah E, Khan MA, Li MY, Hayat T (2020) Backward bifurcation and sensitivity analysis for bacterial meningitis transmission dynamics with a nonlinear recovery rate. Chaos Solitons Fractals 140:110237

Asplin P, Keeling MJ, Mancy R, Hill EM (2024) Epidemiological and health economic implications of symptom propagation in respiratory pathogens: a mathematical modelling investigation. PLoS Comput Biol 20(5):e1012096

Chitnis N, Hyman JM, Cushing JM (2008) Determining important parameters in the spread of malaria through the sensitivity analysis of a mathematical model. Bull Math Biol 70:1272–1296

Crankson MV, Olotu O, Afolabi AS, Abidemi A (2023) Modeling the vaccination control of bacterial meningitis transmission dynamics: a case study. Math Model Control 3(4):416–434

degli Atti MC, Esposito S, Parola L, Ravà L, Gargantini G, Longhi R, working group G (2014) In-hospital management of children with bacterial meningitis in Italy. Ital J Pediatr 40:1–7

Diekmann O, Heesterbeek JAP, Metz JA (1990) On the definition and the computation of the basic reproduction ratio $\mathcal{R}_0$ in models for

infectious diseases in heterogeneous populations. J Math Biol 28:365–382
ELmojtaba IM, Adam S (2017) A mathematical model for meningitis disease. Red Sea Univ J Basic Appl Sci 2(2):467–472
Hadley L, Soeters HM, Cooper LV, Fernandez K, Latt A, Fouda AAB, Trotter C (2024) Modelling control strategies for pneumococcal meningitis outbreaks in the African meningitis belt. Vaccine 42(20):125983
Hinduja A, Tariq A, Adriance S (2019) Intensivecare management of meningitis and encephalitis. Textbook of Neuroanesthesia and Neurocritical Care: Volume II-NeurocriticalCare (2019): 131–144
Ijeh S, Okolo CA, Arowoogun JO, Adeniyi AO, Omotayo O (2024) Predictive modeling for disease outbreaks: a review of data sources and accuracy. Int Med Sci Res J 4(4):406–419
James Peter O, Ojo MM, Viriyapong R, Abiodun Oguntolu F (2022) Mathematical model of measles transmission dynamics using real data from Nigeria. J Differ Equ Appl 28(6):753–770
Kotola BS, Mekonnen TT (2022) Mathematical model analysis and numerical simulation for codynamics of meningitis and pneumonia infection with intervention. Sci Rep 12(1):2639
Madaki UY, Shu'aibu A, Umar MI (2023) Mathematical model for the dynamics of bacterial meningitis (Meningococcal meningitis): a case study of Yobe state specialist hospital, damaturu, nigeria. Gadau J Pure Allied Sci 2(2):113–129
Maseno K (2011) Mathematical model for malaria and meningitis co-infection among children. Appl Math Sci 5(47):2337–2359
Mazamay S, Guégan J-F, Diallo N, Bompangue D, Bokabo E, Muyembe J-J, Taty N, Vita TP, Broutin H (1928) An overview of bacterial meningitis epidemics in Africa from, to 2018 with a focus on epidemics "outside-the-belt''. BMC Infect Dis 21(2021):1–13
Meyfroidt G, Kurtz P, Sonneville R (2020) Critical care management of infectious meningitis and encephalitis. Intensive Care Med 46:192–201. https://doi.org/10.1007/s00134-019-05901-w
Musa SS, Zhao S, Hussaini N, Habib AG, He D (2020) Mathematical modeling and analysis of meningococcal meningitis transmission dynamics. Int J Biomath 13(01):2050006
Myrzakerimova A, Kolesnikova K, Nurmaganbetova M (2024) Use of mathematical modeling tools to support decision-making in medicine. Proc Comput Sci 231:335–340
NC (2024) for Disease Control, Prevention, An update of meningitis outbreak in Nigeria, NCDC Situation Reports. https://ncdc.gov.ng/diseases/sitreps/?cat=6&name=An%20Update%20of%20Meningitis%20Outbreak%20in%20Nigeria
Nigeria Centre for Disease Control (2019) Meningitis, https://ncdc.gov.ng/diseases/factsheet/49. Accessed 27 July 2024
Nyerere N, Mpeshe SC, Ainea N, Ayoade AA, Mgandu FA (2024) Global sensitivity analysis and optimal control of typhoid fever transmission dynamics. Math Model Anal 29(1):141–160
Nyerere N, Liana Y (2024) A mathematical analysis of the effects of control strategies on the transmission dynamics of Chlamydiosis. Decis Anal J 12(2024):100490. https://doi.org/10.1016/j.dajour.2024.100490
Ojo MM, Peter OJ, Goufo EFD, Panigoro HS, Oguntolu FA (2023) Mathematical model for control of tuberculosis epidemiology. J Appl Math Comput 69(1):69–87
Oordt-Speets AM, Bolijn R, van Hoorn RC, Bhavsar A, Kyaw MH (2018) Global etiology of bacterial meningitis: a systematic review and meta-analysis. PLoS ONE 13(6):e0198772
Opoku, Nicholas Kwasi-Do Ohene, et al. Modelling the Transmission Dynamics of Meningitis among High and Low–Risk People in Ghana with Cost-Effectiveness Analysis. Abstr Appl Anal Vol. 2022. No. 1. Hindawi, 2022. https://doi.org/10.1155/2022/9084283
Organization WH et al (2003) Meningococcal meningitis: overview. Wkly Epidemiol Rec Relevé épidémiologique hebdomadaire 78(33):294–296
Peter OJ, Yusuf A, Ojo MM, Kumar S, Kumari N, Oguntolu FA (2022) A mathematical model analysis of meningitis with treatment and vaccination in fractional derivatives. Int J Appl Comput Math 8(3):117
Peter OJ, Panigoro HS, Abidemi A, Ojo MM, Oguntolu FA (2023a) Mathematical model of covid-19 pandemic with double dose vaccination. Acta Biotheor 71(2):9
Peter OJ, Panigoro HS, Ibrahim MA, Otunuga OM, Ayoola TA, Oladapo AO (2023b) Analysis and dynamics of measles with control strategies: a mathematical modeling approach. Int J Dyn Control 11(5):2538–2552
Putz K, Hayani K, Zar FA (2013) Meningitis. Primary care: clinics in office practice 40(3):707–726
Richard DM, Lipsitch M (2024) What's next: using infectious disease mathematical modelling to address health disparities. Int J Epidemiol 53(1):dyad180
Ruoja C, Mayengo M, Nyerere N, Nyabadza F et al (2025) Modeling the influence of fear and patients' attitudes on the transmission dynamics of tuberculosis. Model Earth Syst Environ 11(1):1–16
Saravanan D, Subramanian V, Sundararajan R, Kirubhashankar C et al (2024) Mathematical modelling in the analysis of viral diseases and communicable diseases. In: Revolutionizing the healthcare sector with AI. IGI Global, pp. 273–292
Toaha S, Azis MI et al (2025) Optimal control of transmission dynamics of meningitis disease with vaccination, campaign, and treatment factors. J Adv Res Appl Sci Eng Technol 43(2):21–31
Van den Driessche P (2017) Reproduction numbers of infectious disease models. Infect Dis Model 2(3):288–303
Van den Driessche P, Watmough J (2002) Reproduction numbers and sub-threshold endemic equilibria for compartmental models of disease transmission. Math Biosci 180(1–2):29–48
Verma R, Khanna P (2012) Meningococcal vaccine: a new vaccine to combat meningococcal disease in India. Human Vaccines Immunotherap 8(12):1904–1906
Veronica CM, Olusegun O, Newton A, Sunday AA (2021) Mathematical modeling and stability analyses on the transmission dynamics of bacterial meningitis. J Math Comput Sci 11(6):7384–7413
WHO (2023) Meningitis—who fact sheet, https://www.who.int/health-topics/meningitis#tab=tab_1. Accessed 23 July 2024
Young N, Thomas M (2018) Meningitis in adults: diagnosis and management. Intern Med J 48(11):1294–1307